Electronic Supplementary Material (ESI) for Physical Chemistry Chemical Physics.
This journal is © the Owner Societies 2017

# Electronic Supplementary Information

## Photoinduced dynamics of the hole-transport material H101 in organic solvents and on mesoporous $Al_2O_3$ and $TiO_2$ thin films

*Johannes R. Klein, Mirko Scholz, Kawon Oum* and Thomas Lenzer**

Universität Siegen, Physikalische Chemie, Adolf-Reichwein-Str. 2, 57076 Siegen, Germany,

E-mail: oum@chemie.uni-siegen.de, lenzer@chemie.uni-siegen.de

**Table of contents**

# 1 Analysis of steady-state spectra of H101 in organic solvents

## 1.1. Characteristics of steady-state absorption and fluorescence spectra

Characteristic quantities of the solvent dependent steady-state absorption and fluorescence spectra of neutral H101 are summarised in Table S1. The values are employed in the solvatochromism analysis in Fig. 2(B) and (C) of the main manuscript.

**Table S1** Characteristics of solvent-dependent steady-state absorption and fluorescence spectra of neutral H101 ($S_0 \rightarrow S_1$ transition).

| Solvent | $\lambda_{max}$ [a] (nm) | $\varepsilon_{max}$ [a] ($M^{-1} cm^{-1}$) | $R(n)$ [b] | $\Delta f$ [b] | $\tilde{\nu}_{abs}^{0,0}$ [c] ($cm^{-1}$) | $\tilde{\nu}_{Fl}^{0,0}$ [c] ($cm^{-1}$) | $\Delta\tilde{\nu}_{Stokes}$ ($cm^{-1}$) |
|---|---|---|---|---|---|---|---|
| Acetonitrile | 398.6 | $51600 \pm 700$ | 0.21 | 0.71 | 23640 | 21300 | 2340 |
| Methanol | 398.6 | $49000 \pm 2000$ | 0.20 | 0.71 | 23650 | 21750 | 1900 |
| Ethanol | 400.6 | $53000 \pm 3000$ | 0.22 | 0.67 | 23570 | 21840 | 1730 |
| THF | 404.0 | $55000 \pm 3000$ | 0.25 | 0.44 | 23350 | 21790 | 1560 |
| Chlorobenzene | 408.0 | --- | 0.31 | 0.30 | 23130 | 21520 | 1610 |
| *n*-Hexane | 401.1 | $57000 \pm 4000$ | 0.23 | 0.00 | 23530 | 22460 | 1070 |

[a] Peak of the $S_0 \rightarrow S_1$ absorption band and its absolute absorption coefficient.

[b] Solvent polarity function $\Delta f = R(\varepsilon)-R(n)$ with $R(\varepsilon) = (\varepsilon-1)/(\varepsilon+2)$ and $R(n) = (n^2-1)/(n^2+2)$ using the dielectric constant $\varepsilon$ and the index of refraction $n$ of the respective solvents at room temperature.

[c] Position of the respective 0-0 transitions obtained by fitting a sum of Gaussian functions to the absorption and fluorescence spectra (see Fig. S1(B) and Fig. S1(C). The Stokes shift is then taken as the difference of both values.

## 1.2. Steady-state absorption, emission and excitation spectra in ethanol and acetonitrile

We mentioned in the main text (see Section 3.1) that the fluorescence excitation and absorption spectra were identical for instance in ethanol and acetonitrile. Fig. S1(A) demonstrates this. The excitation spectrum (blue solid line) was recorded for emission at 500 nm and 480 nm for ethanol and acetonitrile, respectively. We overlay the steady-state absorption spectra (red solid line) and show that they are practically identical.

We also mentioned in Section 3.1 that the fluorescence spectra did not show any dependence on the excitation wavelength in the range 300-450 nm. Fig. S1(A) demonstrates this also, for example in ethanol and acetonitrile.

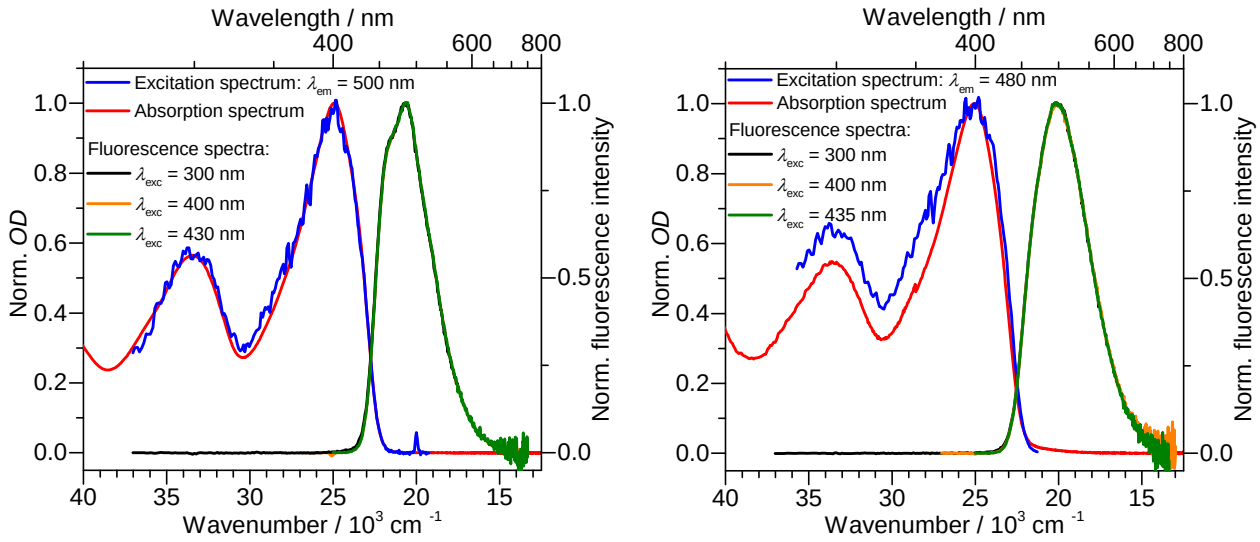


**Fig. S1(A)** Normalised steady-state absorption, excitation and fluorescence spectra of H101 in ethanol (left) and in acetonitrile (right). Excitation wavelengths for the fluorescence emission spectra are indicated in the figure. Excitation spectra are shown as blue solid lines for the emission at 500 nm and 480 nm in ethanol and acetonitrile, respectively.

### 1.3. Peak analysis of steady-state absorption and emission spectra in organic solvents

The $S_0 \rightarrow S_1$ absorption band of H101 peaking at about 400 nm has a shoulder on the longer wavelength side. The emission spectrum shows vibronic structure, which is solvent dependent. For quantifying the Stokes shift, absorption and emission spectra were fitted by a sum of Gaussian functions (see Fig. S1(B) and Fig. S1(C)). The resulting peak position of the 0-0 transition is summarised in Table S1 for each solvent.

### 1.4. Concentration dependence of steady-state absorption spectra in organic solvents

For the transient absorption experiments in organic solvents, we kept the concentration of 0.6-40 μM in order to avoid the optical saturation at 400 nm in our experiment using an optical flow cell with a path length of 0.4-1 mm. In this concentration range, the normalised steady-state absorption spectra were identical. In Fig. S1(D) we compare the normalised absorption spectra with different concentrations of H101 in organic solvents which we used in this work.

(i) *n*-Hexane

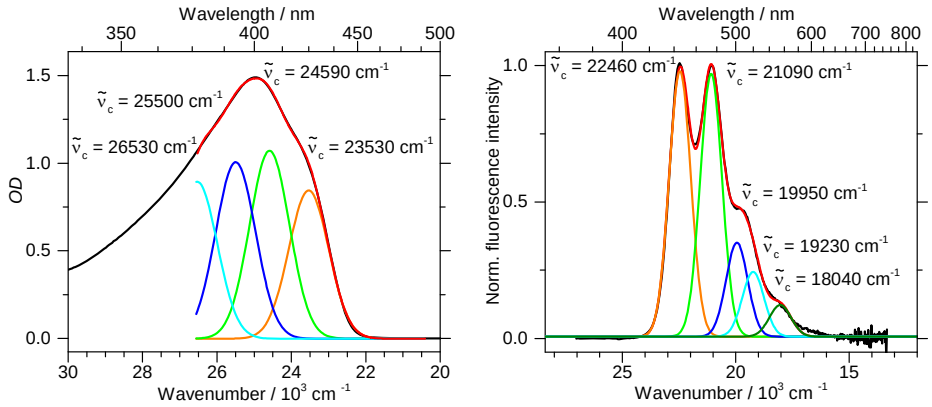


(ii) Chlorobenzene

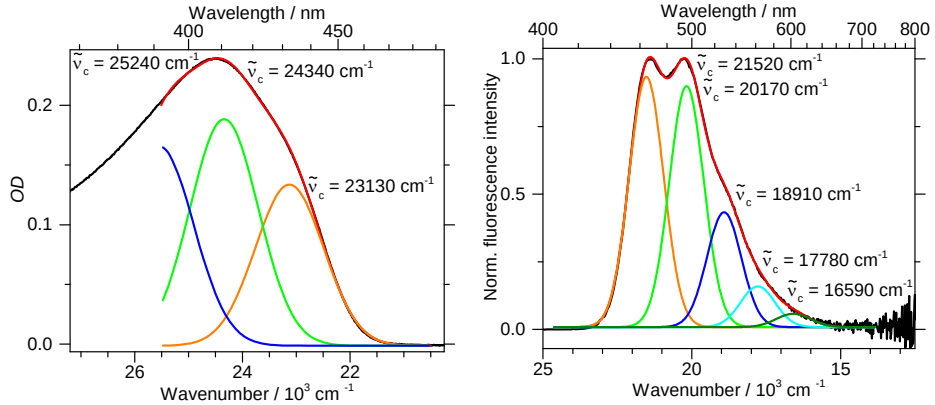


(iii) THF

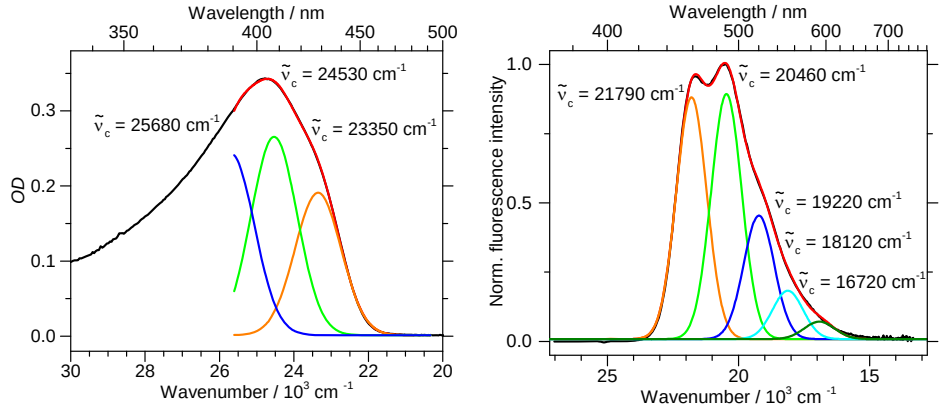


**Fig. S1(B)** Examples of the peak analysis of steady-state absorption and fluorescence spectra of H101 in *n*-hexane, chlorobenzene and THF using a sum of Gaussian functions: (black) experimental data; (red) sum of Gaussian functions; (other colours) individual Gaussian contributions having the same width.

(vi) Ethanol

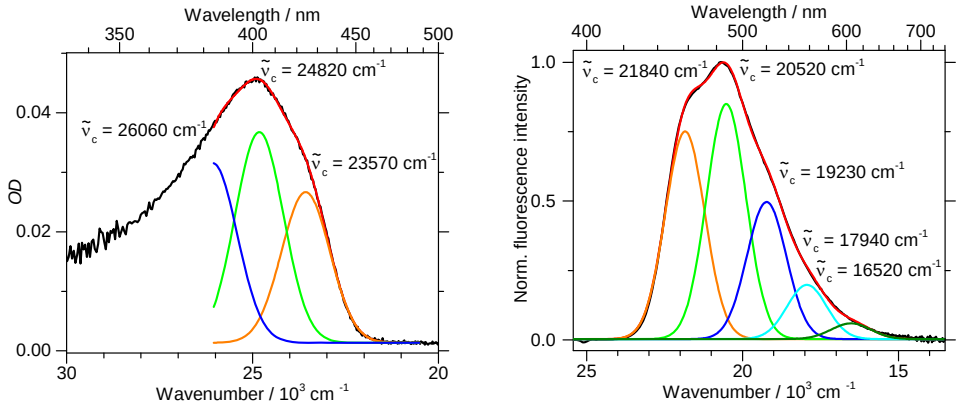


(v) Methanol

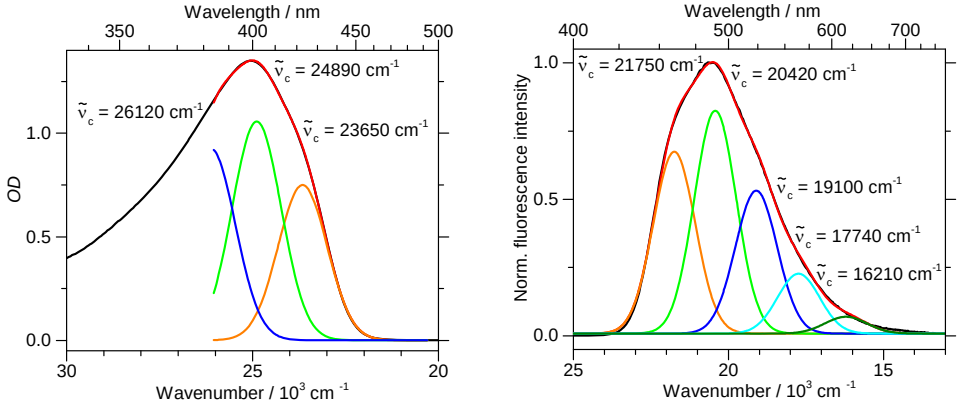


(vi) Acetonitrile

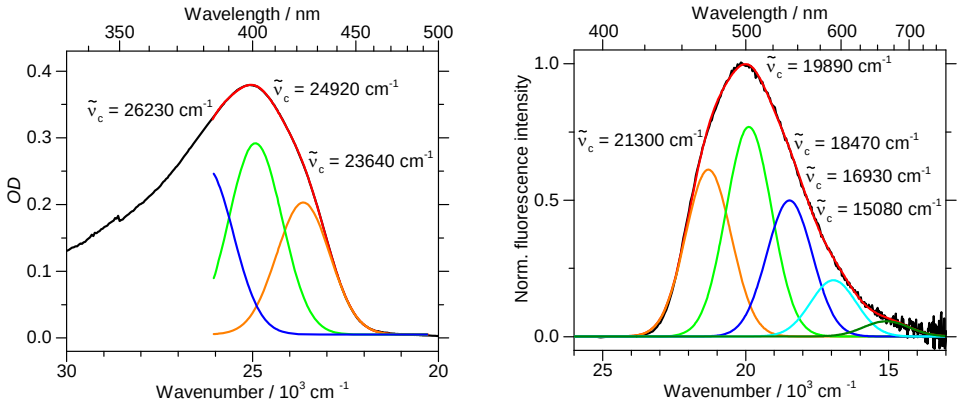


**Fig. S1(C)** Same as Fig. S1(B) but in ethanol, methanol and acetonitrile.

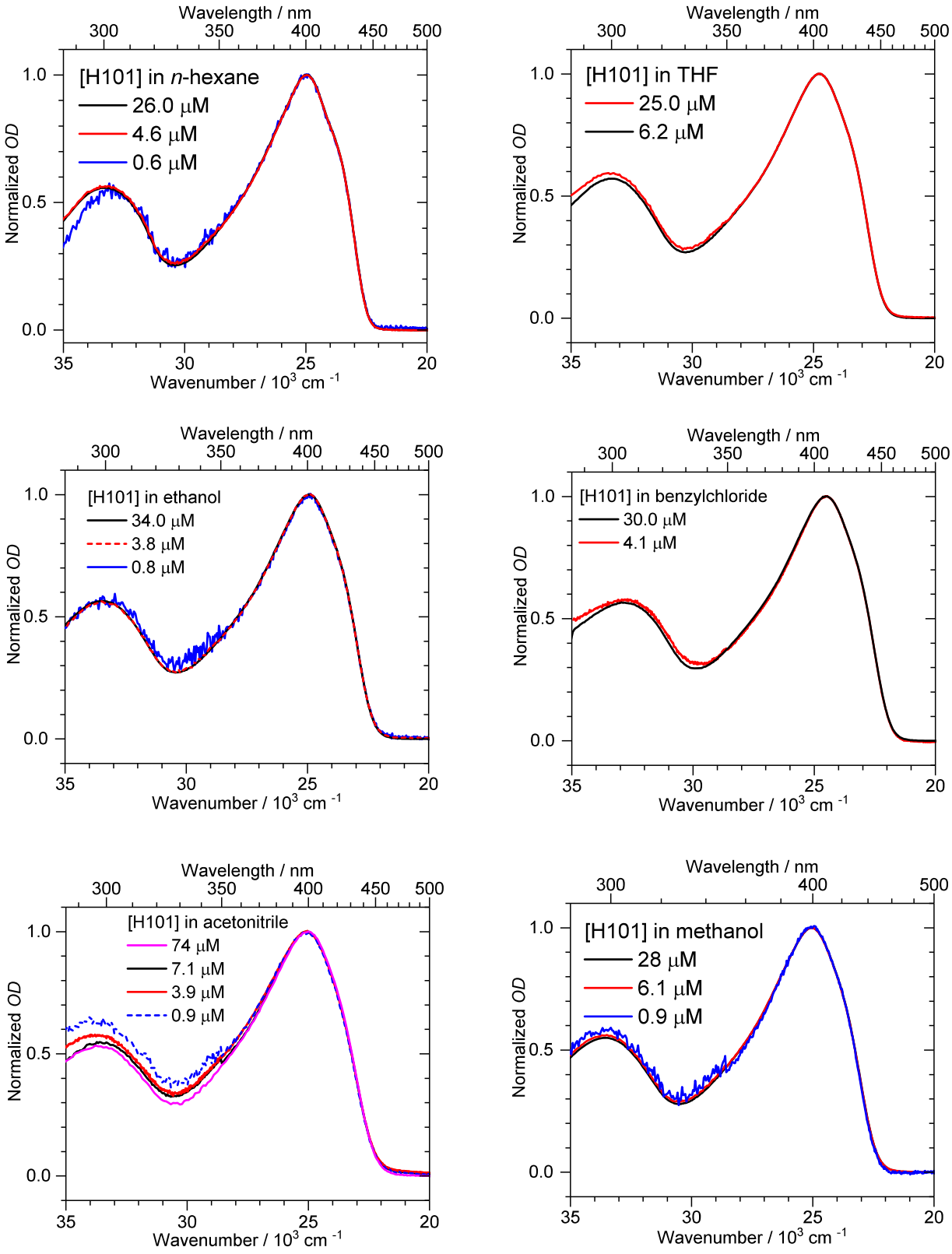


**Fig. S1(D)** Normalised steady-state absorption spectra of H101 with different concentrations in various organic solvents used in this study. The deviation in the deep UV range is due to the difficulties in baseline correction especially at low concentrations.

## 2 Steady-state absorption and fluorescence spectra of H101 on $Al_2O_3$

We also recorded concentration-dependent steady-state absorption and fluorescence spectra of H101 on mesoporous $Al_2O_3$ thin films. These were sensitised by acetonitrile solutions with initial concentrations of H101 in the range 1.5-15 mM. Films with a thickness of 6 and 9 μm were employed. The fluorescence spectra were normalised with respect to their optical density at the excitation wavelength 400 nm. We observed decreasing fluorescence intensity with increasing absorption (Fig. S2). There may be two scenarios to explain this trend: (a) the loss of excited-state population by forming a radical cation – radical anion pair through exciton-splitting,[1] or (b) an increase in polarity of the nearby environment by increasing the dye concentration as previously demonstrated by us for the D49 dye on $Al_2O_3$.[2] From the fact that the fluorescence intensity is not strongly sensitive to solvent polarity in the case of H101 (Fig. 2(A), main manuscript) and also that the fluorescence maxima do not shift appreciably with increasing initial H101 concentration, exciton-splitting is the more likely explanation for the observed fluorescence quenching.

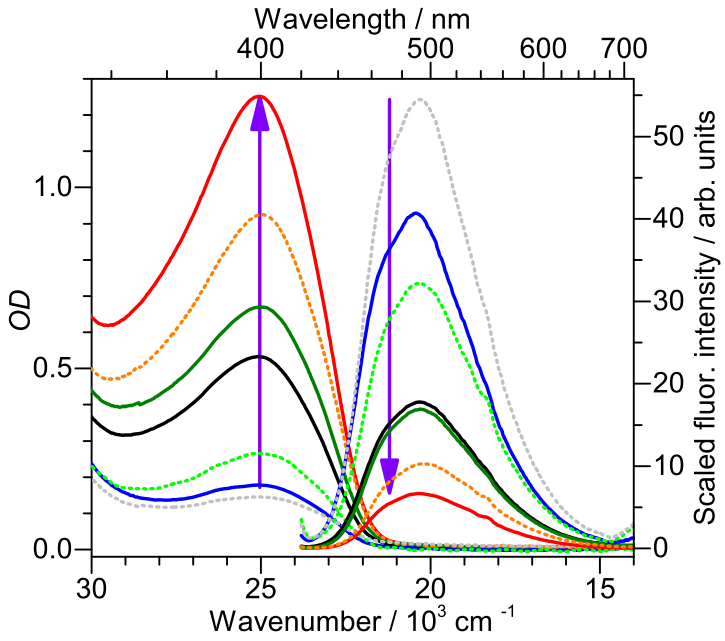


**Fig. S2** Concentration-dependent steady-state absorption and fluorescence spectra of H101 on mesoporous $Al_2O_3$ thin films. The films were sensitised with different concentrations of H101 in acetonitrile in the range 1.5 – 15 mM. Two different thicknesses, 6 and 9 μm, of the mesoporous $Al_2O_3$ thin films were investigated. The fluorescence spectra were normalised to the optical density at 400 nm. The two violet arrows indicate the trend of decreasing fluorescence intensity with increasing H101 absorption.

## 3 Broadband transient absorption spectra, contour plots and kinetics

An example for the solvent correction of the PSCP signals for H101 in THF is shown in Fig. S3. In panel (A) the chirp-corrected PSCP signal for H101 in THF is presented. Panel (B) shows the pure THF solvent signal with two pronounced Stokes and anti-Stokes features of opposite sign, displaced by *ca.* 2900 $cm^{-1}$ relative to the centre of the pump pulse (25000 $cm^{-1}$). They arise from Raman scattering within the pump-probe overlap time and are due to the C-H stretching modes of THF. In addition, there is a smooth background rising toward the UV region which stems from the coherent electronic contribution.[3] The solvent contributions can be largely subtracted to obtain the response of H101, as seen in panel (C): There is only a weak residual absorption below 400 nm due to imperfect solvent signal subtraction. Solvent signatures completely disappear at 60 fs.

Solvent-corrected transient absorption spectra of H101 in THF and methanol are shown in Fig. S4 and S5, respectively, with the same time steps as for H101 in *n*-hexane and acetonitrile (see Fig. 4 and 5 of the main manuscript). As mentioned in the main manuscript, the kinetic behaviour of H101 in these two solvents is "intermediate" between *n*-hexane and acetonitrile (Table 1). The same fast $S_1 \rightarrow S_{1,relaxed}$ relaxation component is present ($\tau_1$ = 1.0 and 1.5 ps, respectively). The SE band of THF still shows vibronic structure but it is less structured than in *n*-hexane (Fig. 4, main manuscript). In methanol the SE band is broad and structureless. According to the TCSPC experiments, the lifetime of $S_{1,relaxed}$ in THF and methanol is 1170 and 1300 ps, respectively. Consequently, ISC from $S_{1,relaxed}$ is still the dominant channel, but the quantum yield drops ($\Phi_{2a}$ = 71 and 68%) relative to *n*-hexane (Table 1). The PSCP results for H101 in all four solvents confirm that triplet formation is reduced when the polarity of the solvent is increased.

The transient absorption spectra of H101 in the four organic solvents and on the $Al_2O_3$ and $TiO_2$ thin films are shown as contour plots in Fig. S6.

Early-time kinetics of H101 for the four solvents (and also for H101 on mesoporous $TiO_2$ and $Al_2O_3$) are shown in Fig. S7. They complement Fig. 6 (main manuscript) which shows the dynamics on long time scales.

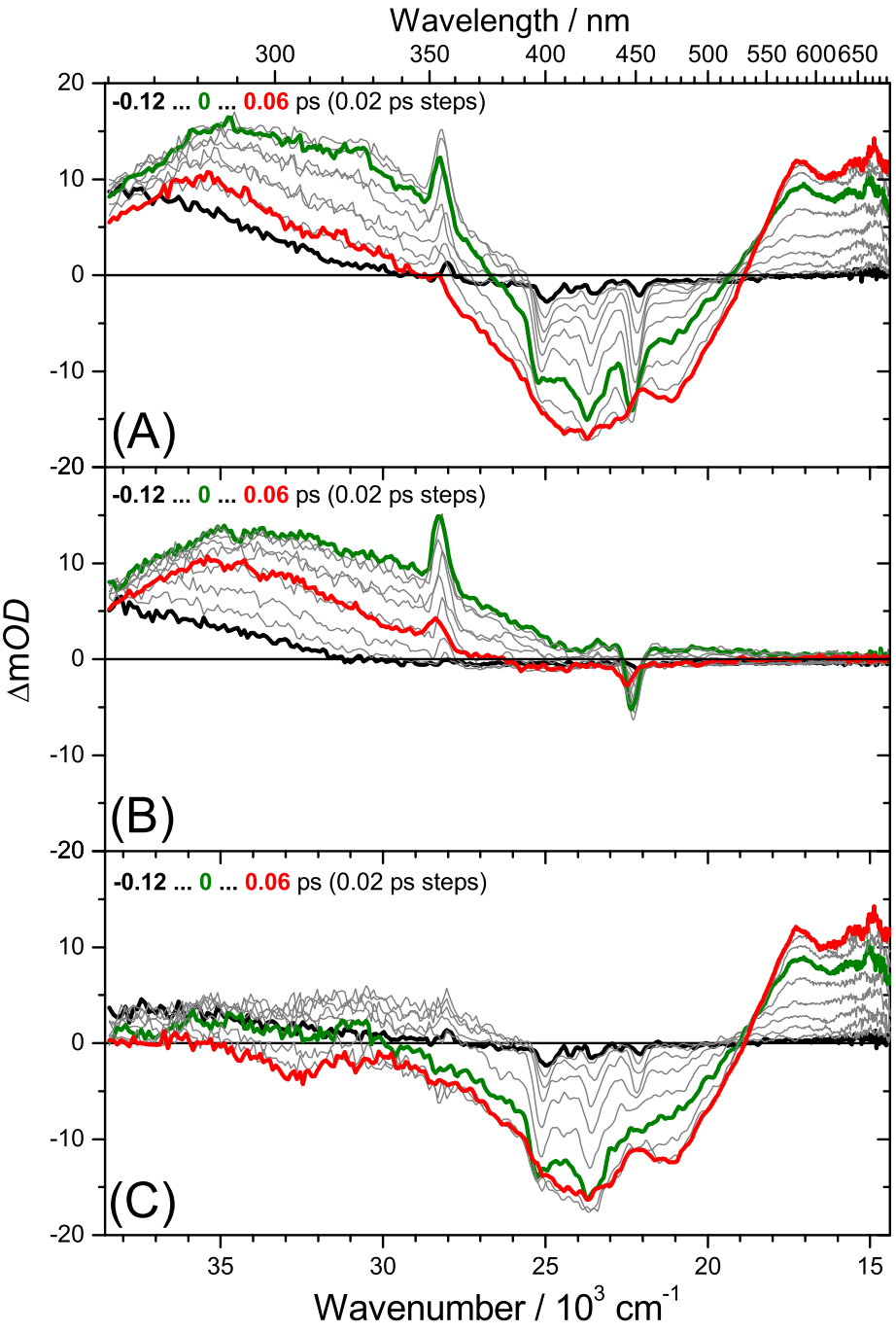


**Fig. S3** PSCP transient absorption spectra of H101 in THF around $t = 0$ ps before (A) and after solvent correction (C), as well as the neat THF solvent signal (B). Photoexcitation was performed at 400 nm. Pump fluence: 190 µJ cm$^{-2}$.

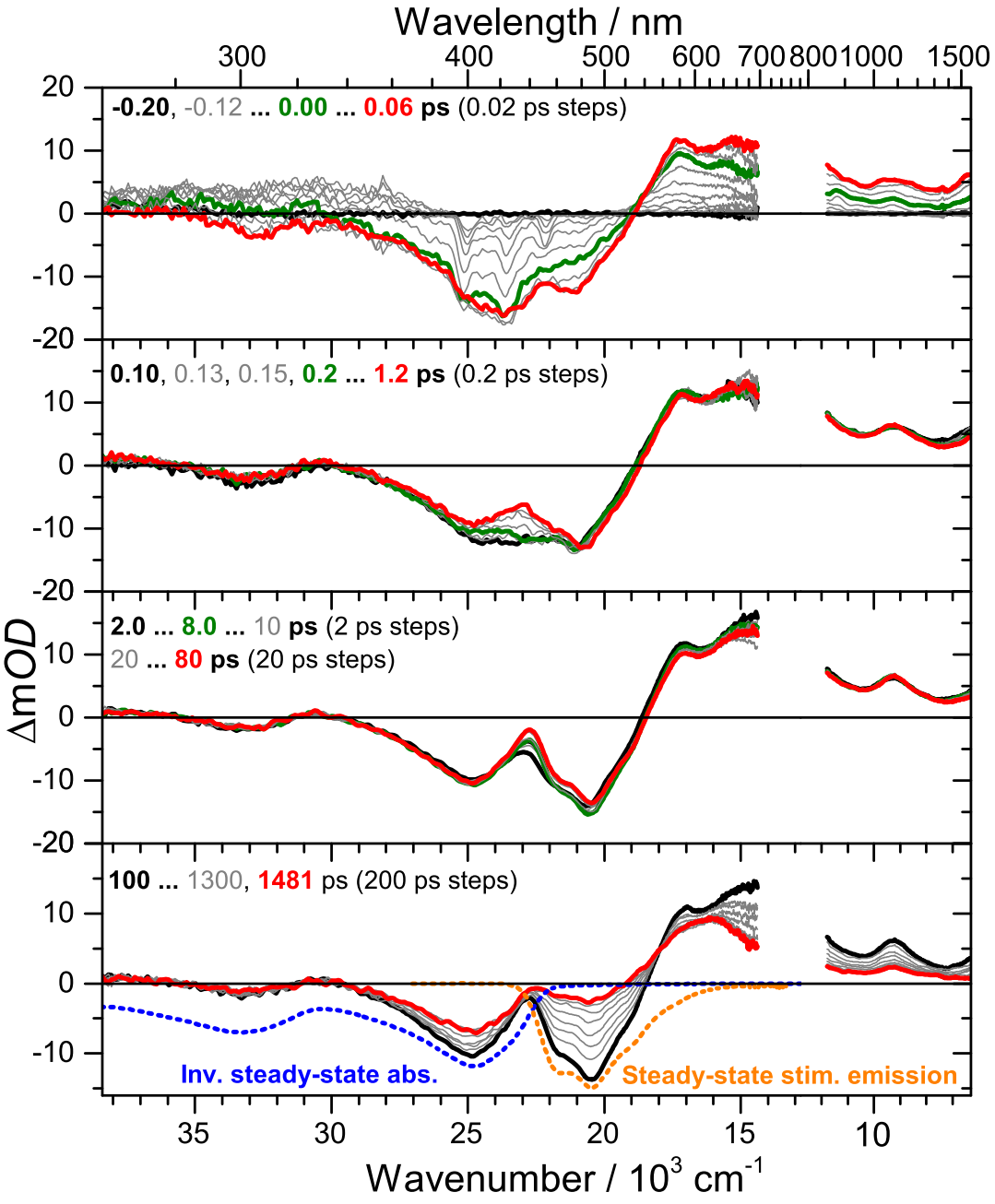


**Fig. S4** Broadband transient PSCP absorption spectra of H101 in THF upon excitation at 400 nm. [H101] = 46 µM. Each panel highlights the time window of particular interest. Fluences are 190 and 260 µJ/cm$^2$ for the UV-Vis and NIR range, respectively. The blue and orange dotted lines in the bottom panel are the inverted steady-state absorption and the steady-state stimulated emission spectra of H101, respectively.

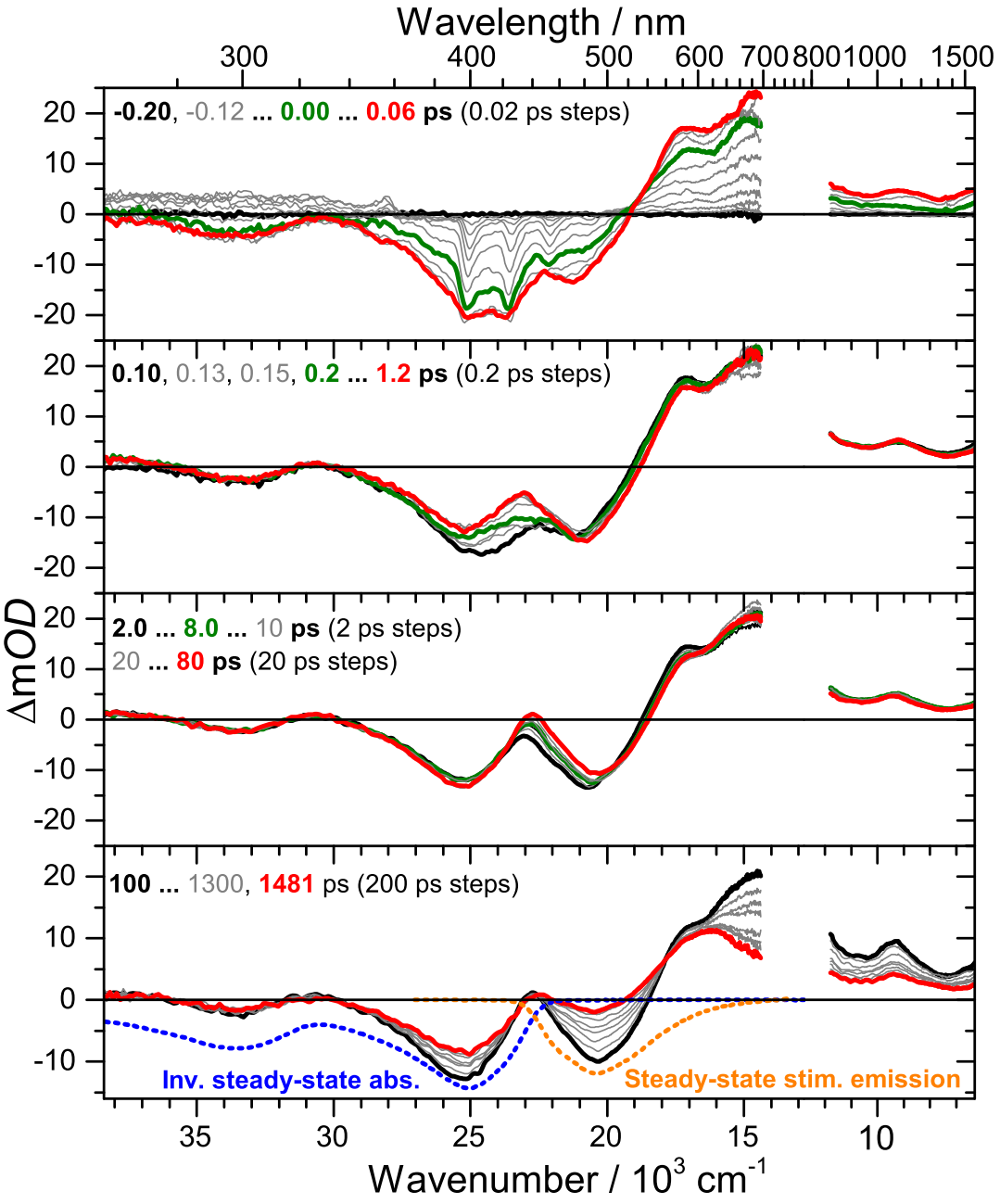


**Fig. S5** Broadband transient PSCP absorption spectra of H101 in methanol upon excitation at 400 nm. [H101] = 43 µM. Each panel highlights the time window of particular interest. Fluences are 106 and 170 µJ/cm$^2$ for the UV-Vis and NIR range, respectively. The blue and orange dotted lines in the bottom panel are the inverted steady-state absorption and the steady-state stimulated emission spectra of H101, respectively.

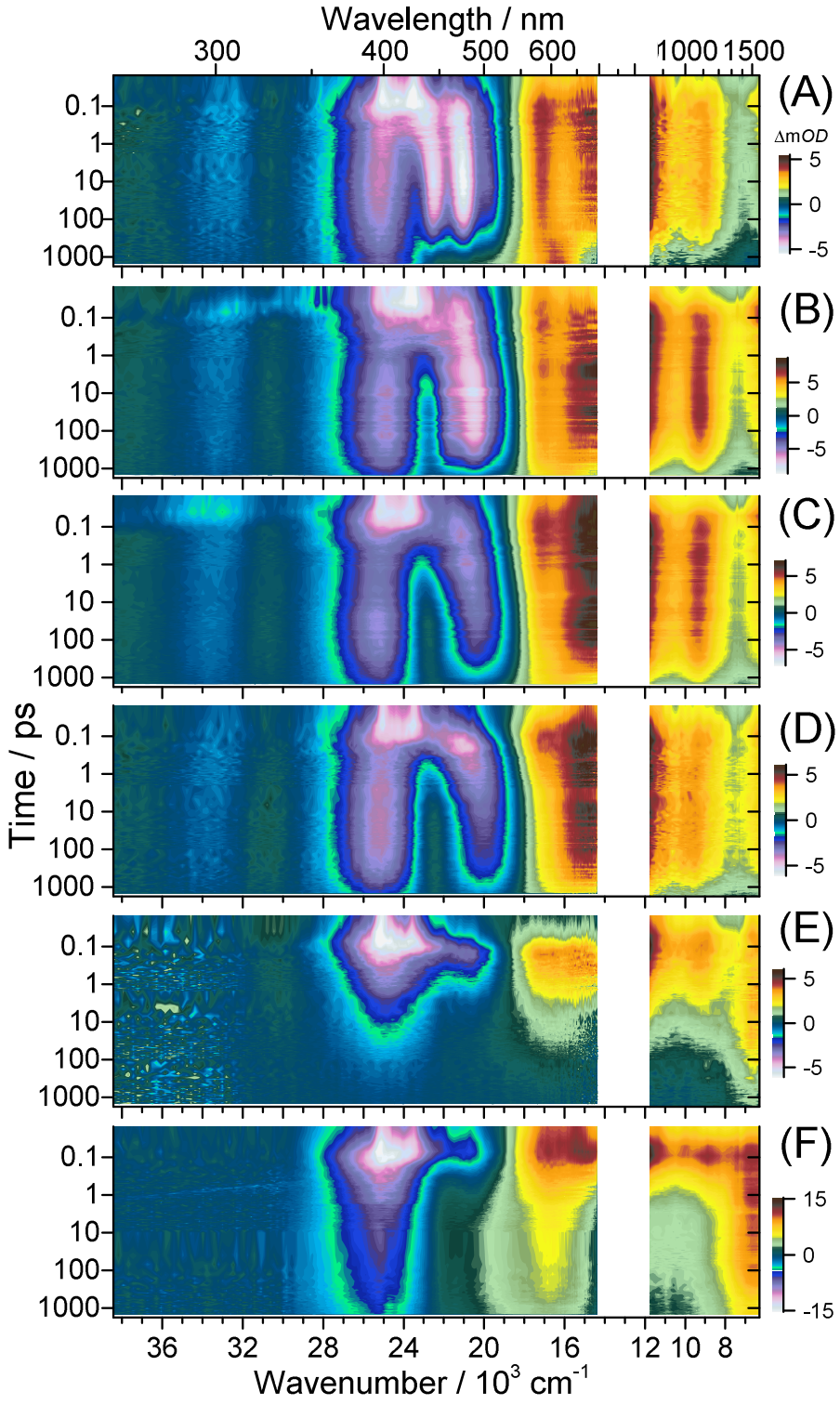


**Fig. S6** Contour plots for broadband transient PSCP spectra of H101 in (A) *n*-hexane, (B) THF, (C) methanol, (D) acetonitrile, and on mesoporous (E) $Al_2O_3$ and (F) $TiO_2$. Pump wavelength: 400 nm.

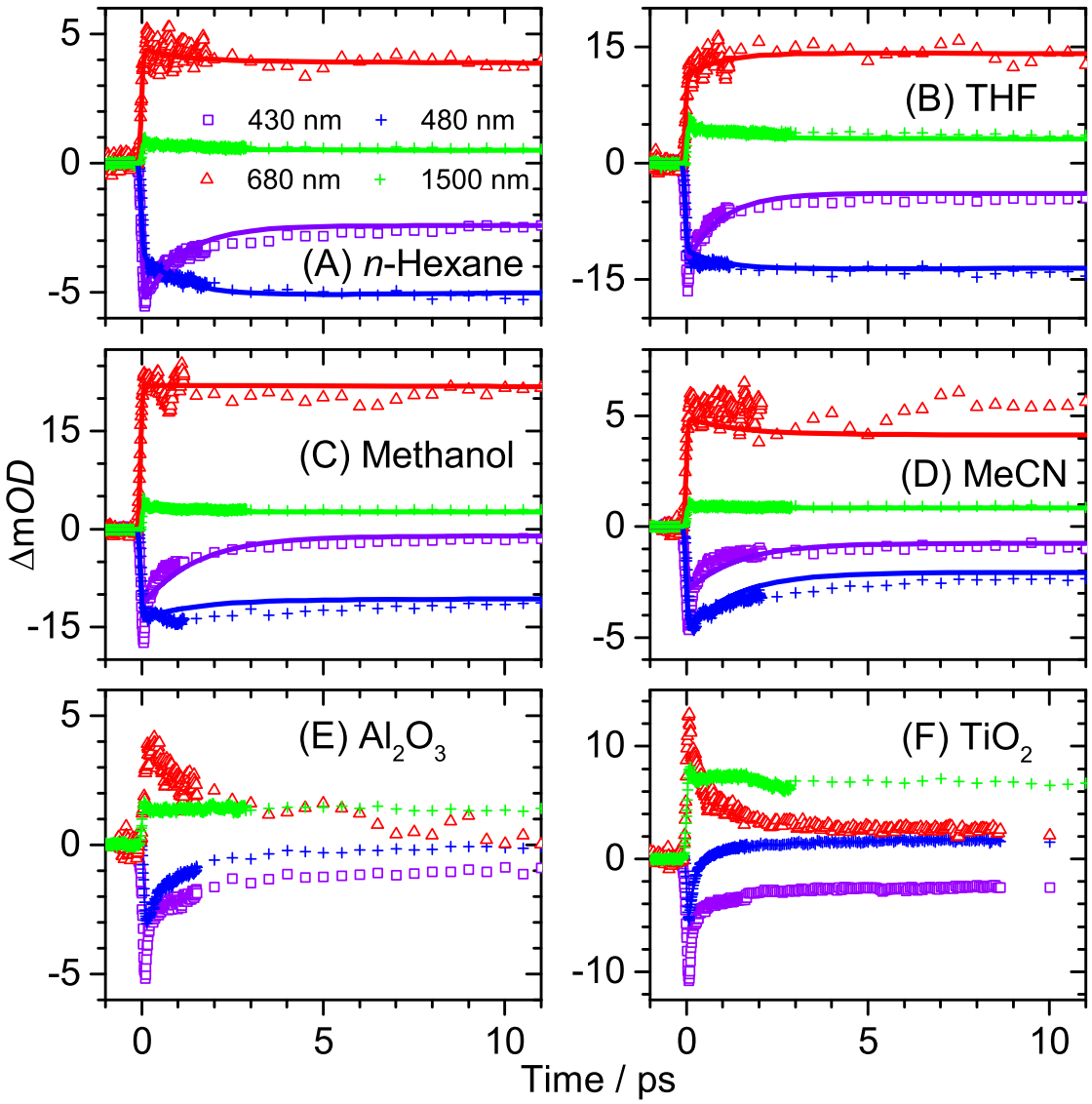


**Fig. S7** Time traces from transient absorption spectra of H101 in organic solvents and on $Al_2O_3$ and $TiO_2$ at the wavelengths 430, 480, 680 and 1500 ($Al_2O_3$: 1300) nm up to 12 ps. Solid lines are the results of the global kinetic analysis. Kinetic traces for pump-probe delays up to 1500 ns are shown in Fig. 6 of the main manuscript.

## 4 Spectral fits for H101 in different solvents

### (a) *n*-Hexane

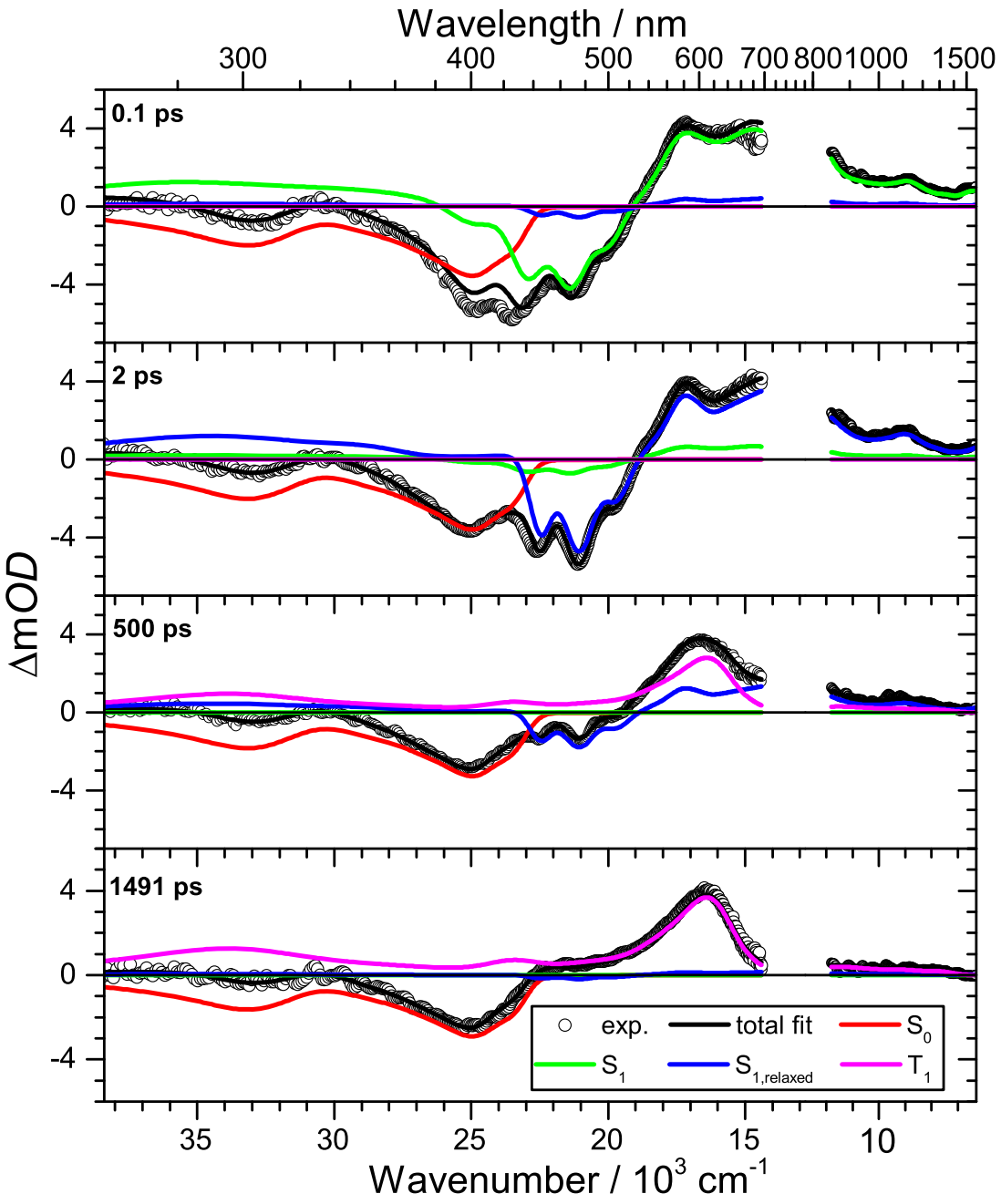


**Fig. S8** Contributions of the different species ($S_0$, $S_1$, $S_{1,relaxed}$ and $T_1$) to the PSCP spectra of H101 in *n*-hexane. Spectral contributions are shown at four selected times.

**(b) THF**

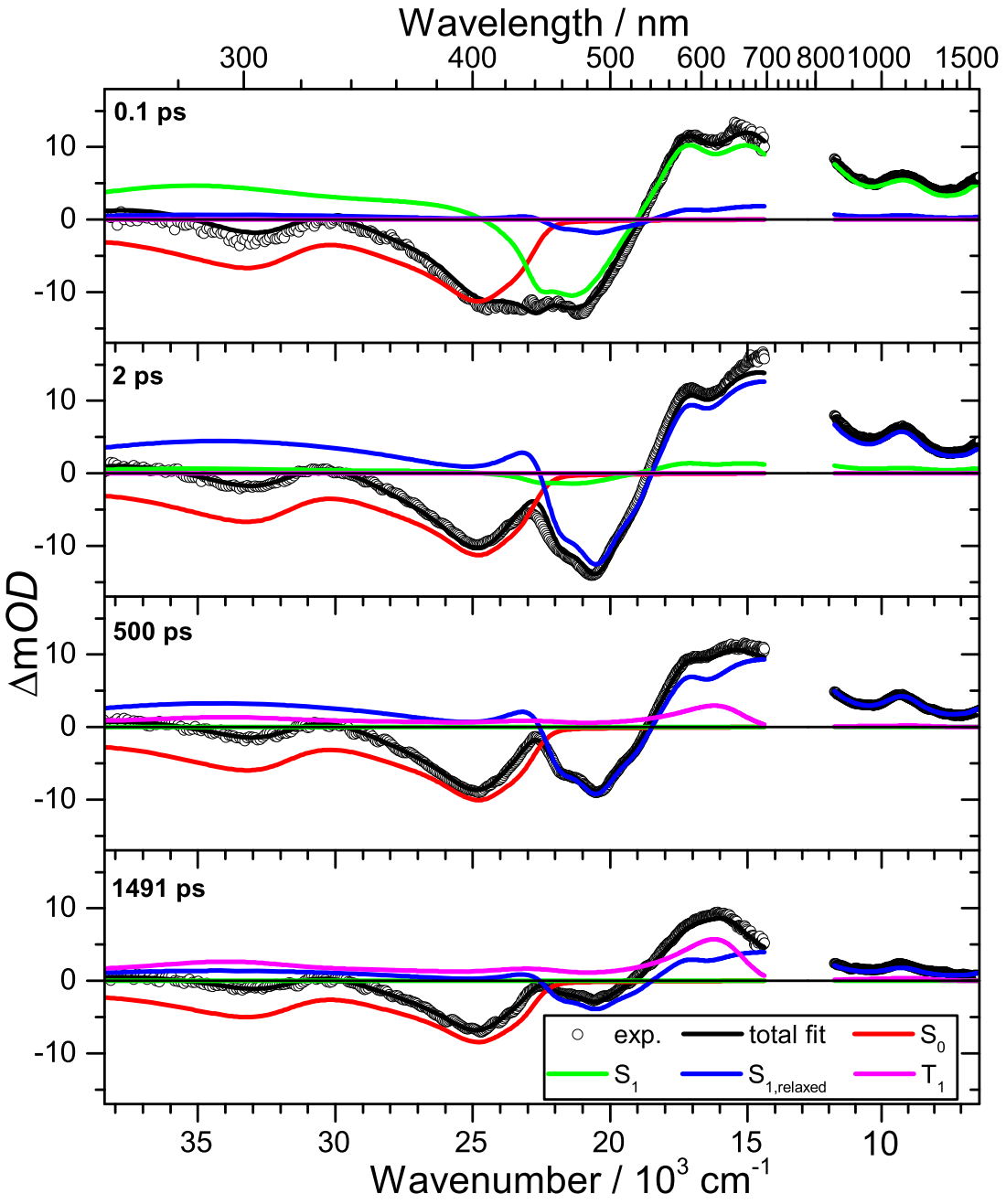


**Fig. S9** Contributions of the different species ($S_0$, $S_1$, $S_{1,relaxed}$ and $T_1$) to the PSCP spectra of H101 in THF. Spectral contributions are shown at four selected times.

**(c) Methanol**

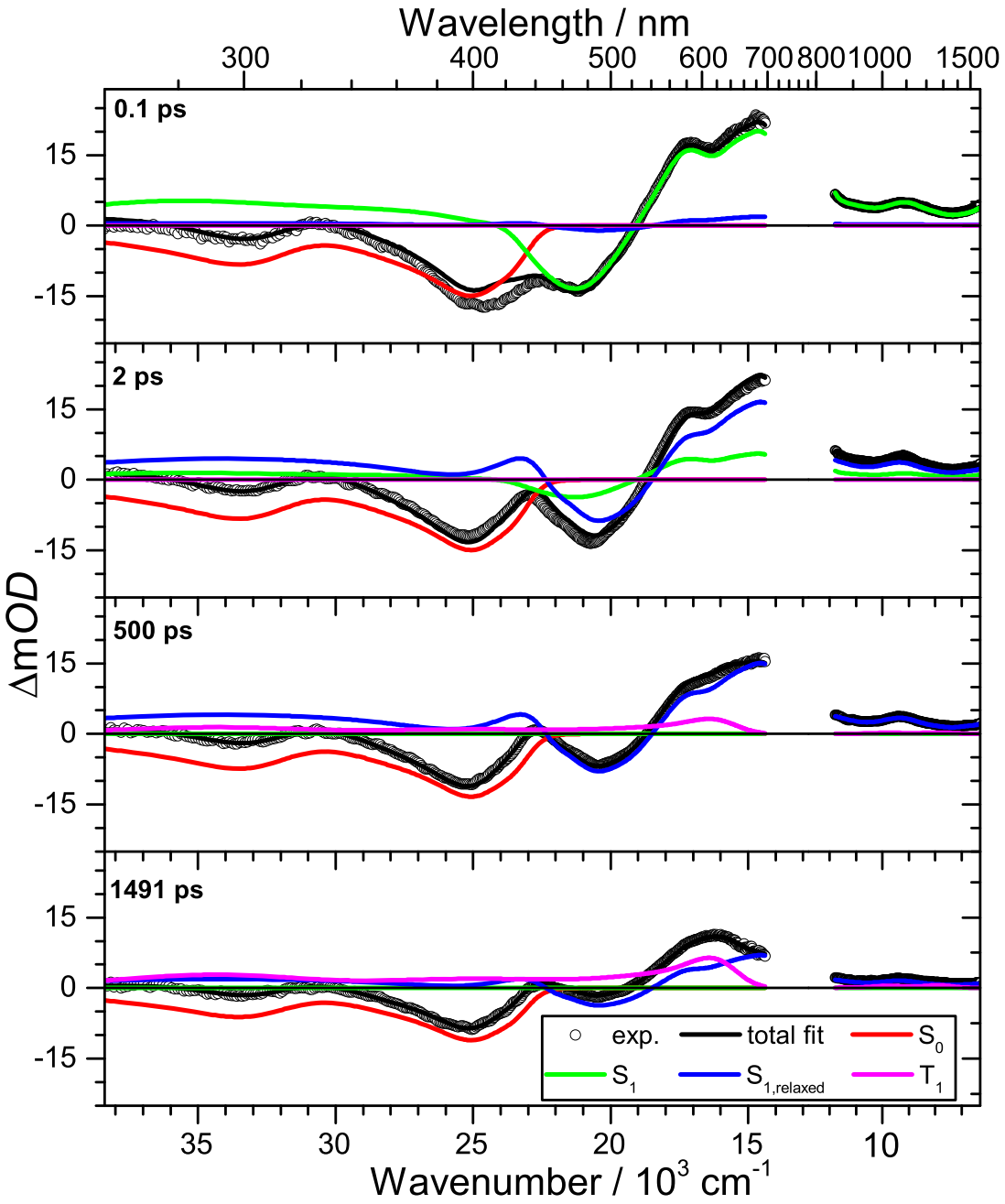


**Fig. S10** Contributions of the different species ($S_0$, $S_1$, $S_{1,relaxed}$ and $T_1$) to the PSCP spectra of H101 in methanol. Spectral contributions are shown at four selected times.

**(d) Acetonitrile**

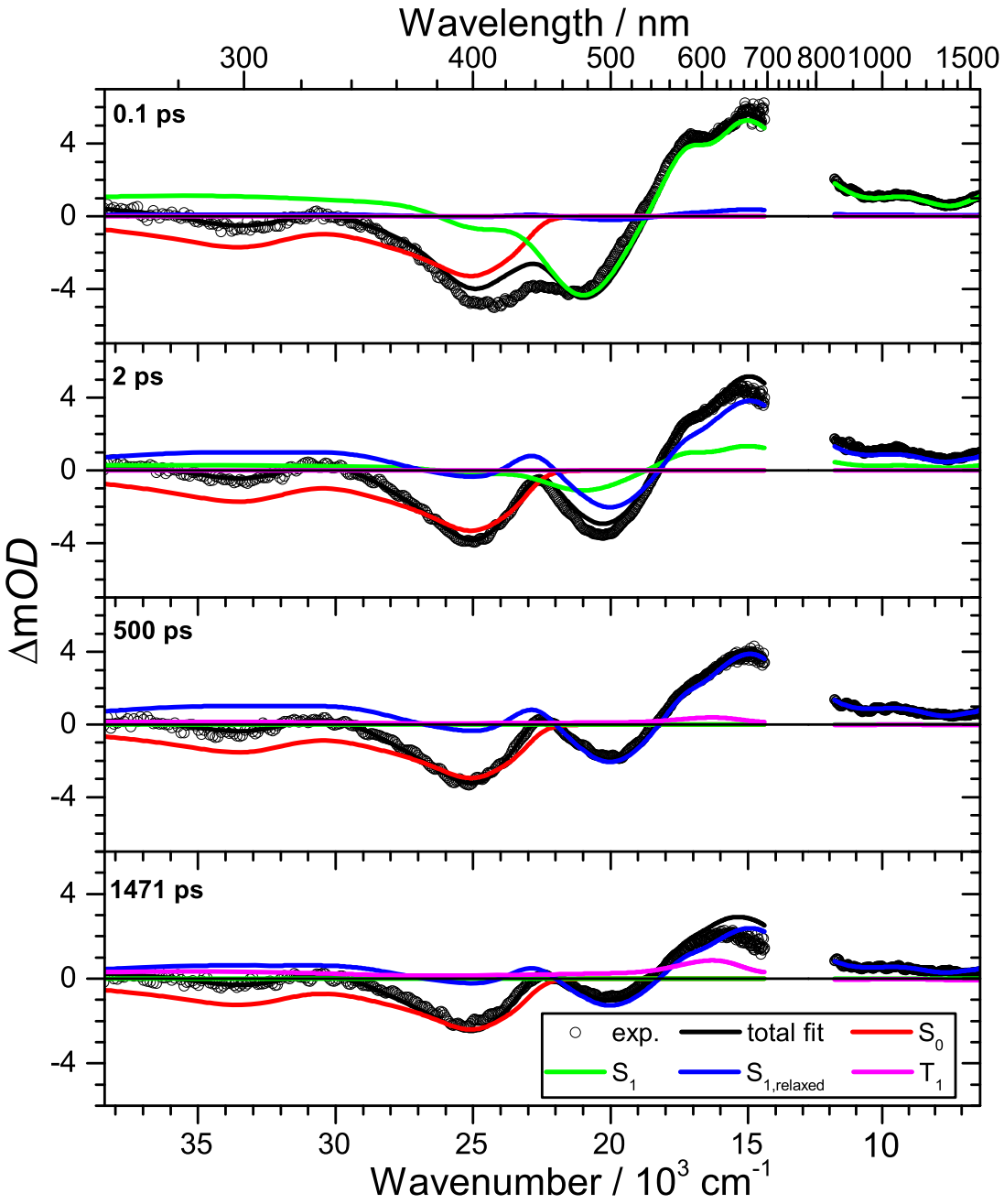


**Fig. S11** Contributions of the different species ($S_0$, $S_1$, $S_{1,relaxed}$ and $T_1$) to the PSCP spectra of H101 in acetonitrile. Spectral contributions are shown at four selected times.

## 5 Analysis of vibronic structure in the absorption and fluorescence spectra

To obtain information regarding the vibronic structure of the absorption and fluorescence spectra of H101 a reduced model system was analysed, *i.e.* H101 with all four methoxy groups replaced by hydrogen ($C_{42}H_{32}N_2O_2S$). These gas-phase calculations were performed using the ORCA 3.0.3 program system.[4] The molecule was optimised using the PBE0 functional, and vibrational frequencies were calculated afterwards. Because only the first electronic transition is of interest here, we used the def2-SV(P) basis[5] for ground and excited state calculations. Subsequently, the program for analysis of electronic spectra orca_asa[6,7] was employed to generate the vibronic spectra in the independent mode displaced harmonic oscillator (IMDHO) approximation.

Figure S12 shows the results for the calculated absorption and fluorescence spectra at 0 (black) and 298 K (red). The spacing and shape of the vibronic main progression in the experimental fluorescence spectrum (blue) are well described. Only the relative peak intensities differ. The calculated absorption spectrum at 298 K shows more structure than predicted by the calculations, but still the peaks are in the correct position. A tentative explanation could be that several conformers contribute to the experimental absorption spectrum at 300 K (which washes out the vibrational structure), whereas fluorescence predominantly stems from one dominant conformer ("$S_{1,relaxed}$" in the main manuscript) giving rise to the sharper emission peaks. The calculations at 0 K lead to the expected further sharpening of the spectrum.

The calculations identify five main vibrational modes with the unscaled frequencies 1517, 1594, 1637, 1689 and 1701 $cm^{-1}$ which are responsible for the vibronic structure. They all involve substantial aromatic C=C ring breathing contributions in the thiophenyl and TAA units.

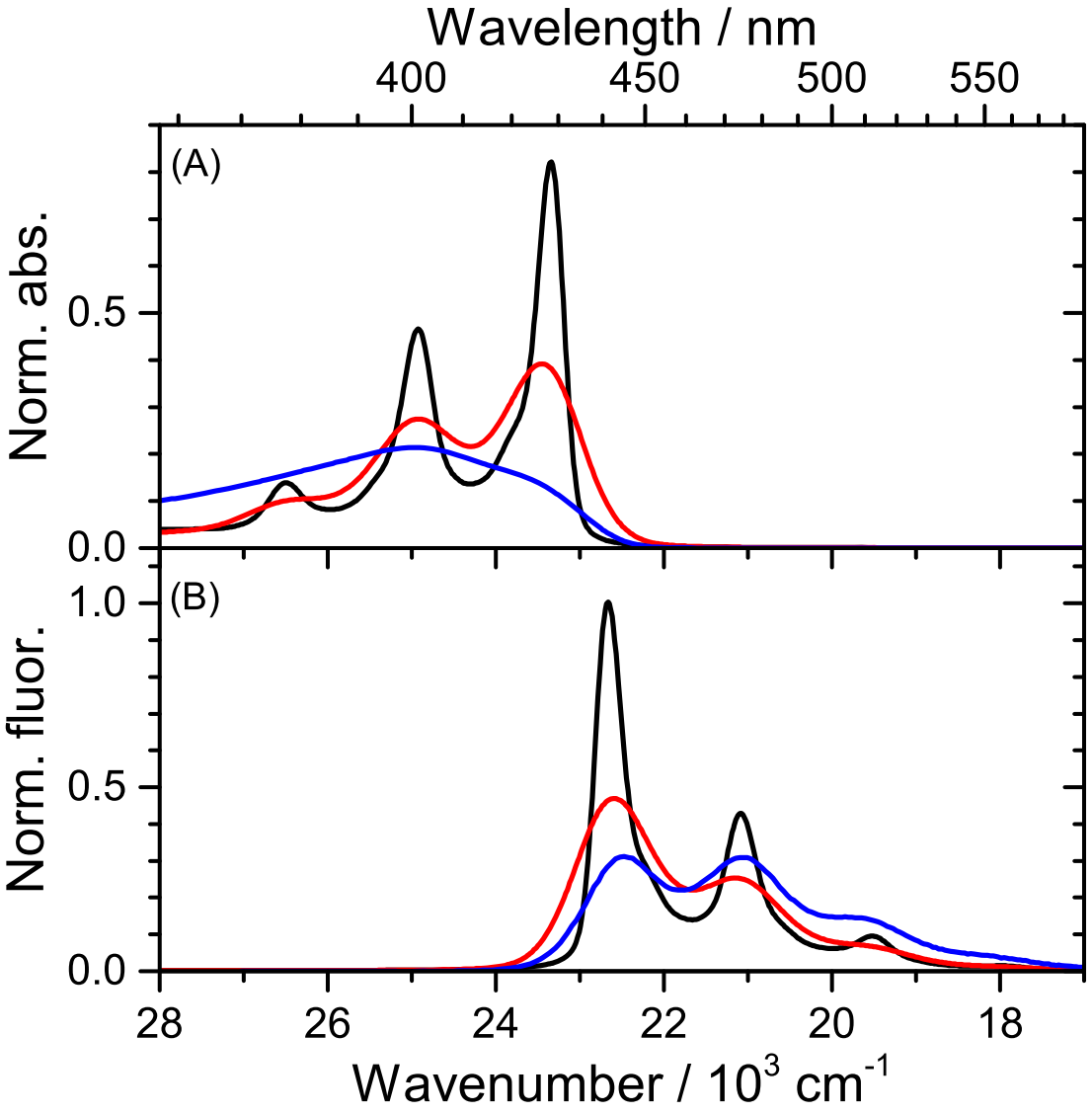


**Fig. S12** Area-normalised absorption (A) and fluorescence (B) spectra for a H101 model system without methoxy substituents. (Black) Simulated spectra for $T$ = 0 K. (Red) Simulated spectra for $T$ = 298 K. The blue lines are the corresponding experimental spectra of H101 in *n*-hexane from Fig. 2 in the main manuscript.

## 6 Difference electron densities from DFT/TDDFT calculations

Figure S13 shows difference electron densities calculated from the Mulliken charges of the $H101^{\bullet+}$ radical cation and neutral H101 (top) as well as the $H101^{\bullet-}$ radical anion and neutral H101 (bottom) for vacuum conditions. Both plots suggest that the excess charge is mainly delocalised over the thiophenyl ring of the EDOT moiety and the adjacent aryl rings of the TAA units.

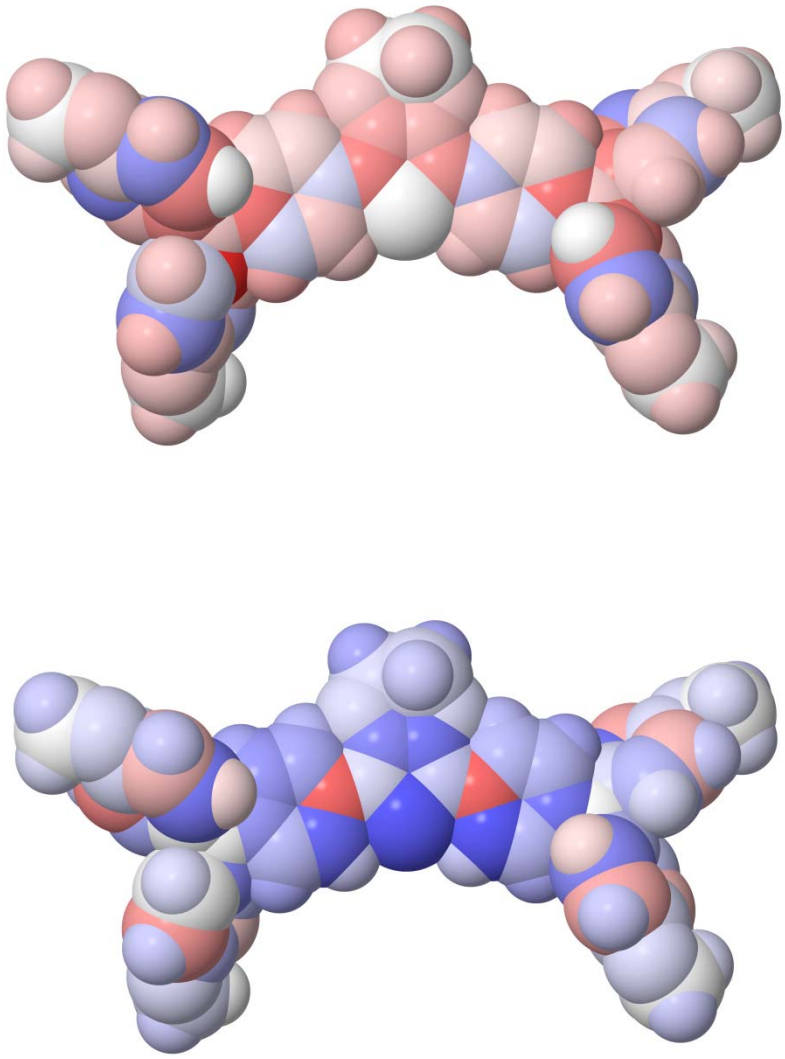

**Fig. S13** Difference electron density of the radical cation $H101^{\bullet+}$ (top) and the radical anion $H101^{\bullet-}$ (bottom) relative to neutral H101. Red colours indicate more positive charge whereas blue colours correspond to more negative charge. View from the top onto the plane of the thiophenyl group.

# 7 Electronic transitions of H101, $H101^{\bullet+}$, $H101^{\bullet-}$ and $H101^{2+}$

**Table S2** Wavenumber $\tilde{\nu}$ and oscillator strength $f$ from DFT/TDDFT calculations in vacuum and acetonitrile (MeCN) for the **transitions of neutral H101 starting from $S_0$ (optimised $S_0$ geometry)**. "S" and "T" in the columns "C" denote the character of the transition, *i.e.* if it is a $S_0 \rightarrow S_n$ or an optically dark $S_0 \rightarrow T_n$ transition, respectively. "Conformer 1" (point group $C_1$) and "Conformer 2" (point group $C_2$) are two different rotamers differing only in the relative rotation of the TAA groups. They are very close in Gibbs free enthalpy (*ca.* 0.05 kJ $mol^{-1}$) and will be both populated at 300 K. The values show that the transition energies of both conformers are also very close, and therefore we only deal with "Conformer 1".

| | **Conformer 1** | | | | | | **Conformer 2** | | | | | |
|---|---|---|---|---|---|---|---|---|---|---|---|---|
| **n** | **Vacuum** | | | **MeCN** | | | **Vacuum** | | | **MeCN** | | |
| | $\tilde{\nu}$ / $cm^{-1}$ | $f$ | **C** | $\tilde{\nu}$ / $cm^{-1}$ | $f$ | **C** | $\tilde{\nu}$ / $cm^{-1}$ | $f$ | **C** | $\tilde{\nu}$ / $cm^{-1}$ | $f$ | **C** |
| 1 | 18275 | 0.00 | T | 24498 | 1.87 | S | 18240 | 0.00 | T | 18133 | 0.00 | T |
| 2 | 24056 | 0.00 | T | 28877 | 0.12 | S | 24180 | 0.00 | T | 23833 | 0.00 | T |
| 3 | 25388 | 1.85 | S | 29882 | 0.02 | S | 25505 | 1.91 | S | 24556 | 1.93 | S |
| 4 | 26054 | 0.00 | T | 29972 | 0.05 | S | 26200 | 0.00 | T | 26387 | 0.00 | T |
| 5 | 26202 | 0.00 | T | 33921 | 0.15 | S | 26214 | 0.00 | T | 26408 | 0.00 | T |
| 6 | 27345 | 0.00 | T | 34072 | 0.09 | S | 27400 | 0.00 | T | 27623 | 0.00 | T |
| 7 | 27401 | 0.00 | T | 34212 | 0.22 | S | 27407 | 0.00 | T | 27628 | 0.00 | T |
| 8 | 27988 | 0.00 | T | 34981 | 0.09 | S | 28112 | 0.00 | T | 27928 | 0.00 | T |
| 9 | 29390 | 0.00 | T | 35141 | 0.13 | S | 29390 | 0.00 | T | 29130 | 0.12 | S |
| 10 | 29694 | 0.06 | S | 35479 | 0.21 | S | 29780 | 0.05 | S | 29141 | 0.00 | T |
| 11 | 29846 | 0.06 | S | 35751 | 0.01 | S | 29848 | 0.05 | S | 30011 | 0.02 | S |
| 12 | 30070 | 0.00 | T | 35965 | 0.03 | S | 30042 | 0.00 | T | 30023 | 0.05 | S |
| 13 | 30094 | 0.03 | S | 36409 | 0.00 | S | 30198 | 0.00 | T | 30339 | 0.00 | T |
| 14 | 30247 | 0.00 | T | 36596 | 0.01 | S | 30374 | 0.05 | S | 30471 | 0.00 | T |
| 15 | 30431 | 0.00 | T | 36687 | 0.04 | S | 30533 | 0.00 | T | 30512 | 0.00 | T |
| 16 | 30635 | 0.00 | T | 37002 | 0.14 | S | 30594 | 0.00 | T | 30554 | 0.00 | T |
| 17 | 31430 | 0.00 | T | 37522 | 0.09 | S | 31447 | 0.00 | T | 31401 | 0.00 | T |
| 18 | 31623 | 0.00 | T | 37673 | 0.01 | S | 31874 | 0.00 | T | 31705 | 0.00 | T |
| 19 | 32451 | 0.00 | T | 39370 | 0.00 | S | 32579 | 0.00 | T | 32467 | 0.00 | T |
| 20 | 33896 | 0.20 | S | 39957 | 0.00 | S | 33763 | 0.19 | S | 33919 | 0.20 | S |
| 21 | 34083 | 0.20 | S | - | - | - | 33786 | 0.16 | S | 34026 | 0.17 | S |
| 22 | 34205 | 0.00 | T | - | - | - | 34305 | 0.02 | S | 34131 | 0.00 | T |
| 23 | 34243 | 0.01 | S | - | - | - | 34355 | 0.00 | T | 34148 | 0.03 | S |
| 24 | 35128 | 0.04 | S | - | - | - | 35087 | 0.05 | S | 35214 | 0.09 | S |
| 25 | 35257 | 0.05 | S | - | - | - | 35136 | 0.00 | S | 35344 | 0.07 | S |
| 26 | 35328 | 0.00 | T | - | - | - | 35247 | 0.00 | T | 35533 | 0.27 | S |
| 27 | 35420 | 0.00 | T | - | - | - | 35336 | 0.00 | T | 35666 | 0.00 | T |
| 28 | 35473 | 0.10 | S | - | - | - | 35362 | 0.02 | S | 35680 | 0.01 | S |
| 29 | 35570 | 0.05 | S | - | - | - | 35548 | 0.11 | S | 35705 | 0.00 | T |
| 30 | 35698 | 0.00 | T | - | - | - | 35644 | 0.00 | T | 35768 | 0.01 | S |
| 31 | 35964 | 0.03 | S | - | - | - | 36039 | 0.02 | S | 36127 | 0.00 | T |
| 32 | 35986 | 0.00 | T | - | - | - | 36048 | 0.00 | T | 36340 | 0.00 | T |
| 33 | 36040 | 0.11 | S | - | - | - | 36292 | 0.10 | S | 36585 | 0.02 | S |
| 34 | 36378 | 0.00 | S | - | - | - | 36364 | 0.01 | S | 36591 | 0.01 | S |
| 35 | 36428 | 0.00 | S | - | - | - | 36452 | 0.00 | S | 36786 | 0.07 | S |
| 36 | 36524 | 0.01 | S | - | - | - | 36528 | 0.02 | S | 37056 | 0.11 | S |
| 37 | 37406 | 0.04 | S | - | - | - | 37253 | 0.04 | S | 37479 | 0.05 | S |
| 38 | 37726 | 0.05 | S | - | - | - | 37737 | 0.06 | S | 37748 | 0.06 | S |
| 39 | 37956 | 0.05 | S | - | - | - | 38039 | 0.05 | S | 39299 | 0.00 | S |
| 40 | 38733 | 0.03 | S | - | - | - | 38621 | 0.03 | S | 40062 | 0.00 | S |

**Table S3** Wavenumber $\tilde{\nu}$ and oscillator strength $f$ from DFT/TDDFT calculations in vacuum and acetonitrile (MeCN) for the **$S_0 \rightarrow S_n$ transitions of neutral H101 starting from $S_0$ (optimised $S_1$ geometry)** and for the **$T_1 \rightarrow T_n$ transitions of neutral H101**.

| n | $S_0 \rightarrow S_n$ (optimised $S_1$ geometry) | | | | $T_1 \rightarrow T_n$ | | | |
|---|---|---|---|---|---|---|---|---|
| | Vacuum | | MeCN | | Vacuum | | MeCN | |
| | $\tilde{\nu}$ / cm$^{-1}$ | $f$ | $\tilde{\nu}$ / cm$^{-1}$ | $f$ | $\tilde{\nu}$ / cm$^{-1}$ | $f$ | $\tilde{\nu}$ / cm$^{-1}$ | $f$ |
| 1 | 22010 | 1.93 | 21033 | 1.95 | 12782 | 0.31 | 11695 | 0.53 |
| 2 | 26522 | 0.07 | 25660 | 0.08 | 16421 | 0.19 | 15566 | 0.03 |
| 3 | 28967 | 0.02 | 29014 | 0.03 | 16835 | 0.02 | 16125 | 0.25 |
| 4 | 29072 | 0.04 | 29088 | 0.05 | 18843 | 0.01 | 19047 | 0.71 |
| 5 | 32265 | 0.22 | 31542 | 0.17 | 18953 | 0.01 | 19293 | 0.34 |
| 6 | 32546 | 0.06 | 32257 | 0.06 | 19750 | 1.42 | 19334 | 0.22 |
| 7 | 33172 | 0.14 | 33198 | 0.17 | 22445 | 0.01 | 22360 | 0.00 |
| 8 | 33303 | 0.19 | 33282 | 0.23 | 23329 | 0.01 | 24344 | 0.01 |
| 9 | 34431 | 0.01 | 34517 | 0.12 | 23555 | 0.01 | 24475 | 0.01 |
| 10 | 34668 | 0.04 | 34727 | 0.17 | 23721 | 0.01 | 24782 | 0.01 |
| 11 | 34804 | 0.08 | 35093 | 0.05 | 24225 | 0.01 | 24961 | 0.02 |
| 12 | 34904 | 0.06 | 35147 | 0.13 | 24983 | 0.01 | 25312 | 0.03 |
| 13 | 35118 | 0.06 | 35282 | 0.03 | 25139 | 0.03 | 25844 | 0.54 |
| 14 | 35435 | 0.00 | 35429 | 0.03 | 25475 | 0.01 | 26310 | 0.03 |
| 15 | 35651 | 0.04 | 35678 | 0.03 | 26482 | 0.55 | 26408 | 0.03 |
| 16 | 35723 | 0.00 | 35830 | 0.06 | 26957 | 0.01 | 26574 | 0.01 |
| 17 | 36008 | 0.11 | 36575 | 0.01 | 27046 | 0.07 | 26719 | 0.00 |
| 18 | 36344 | 0.01 | 36768 | 0.06 | 28315 | 0.01 | 27592 | 0.02 |
| 19 | 37132 | 0.03 | 38172 | 0.00 | 28469 | 0.03 | 27615 | 0.04 |
| 20 | 37458 | 0.03 | 38198 | 0.03 | 28539 | 0.00 | 27804 | 0.04 |

**Table S4** Wavenumber $\tilde{\nu}$ and oscillator strength $f$ from DFT/TDDFT calculations in vacuum and acetonitrile (MeCN) for the **$D_0 \rightarrow D_n$ transitions of the radical cation H101$^{\bullet+}$ and the radical anion H101$^{\bullet-}$**.

| n | $D_0 \rightarrow D_n$ (radical cation H101$^{\bullet+}$) | | | | $D_0 \rightarrow D_n$ (radical anion H101$^{\bullet-}$) | | | |
|---|---|---|---|---|---|---|---|---|
| | Vacuum | | MeCN | | Vacuum | | MeCN | |
| | $\tilde{\nu}$ / cm$^{-1}$ | $f$ | $\tilde{\nu}$ / cm$^{-1}$ | $f$ | $\tilde{\nu}$ / cm$^{-1}$ | $f$ | $\tilde{\nu}$ / cm$^{-1}$ | $f$ |
| 1 | 8369 | 1.23 | 7759 | 1.17 | 4723 | 0.00 | 10355 | 0.00 |
| 2 | 13539 | 0.04 | 13557 | 0.05 | 4785 | 0.00 | 10590 | 0.00 |
| 3 | 16906 | 0.00 | 15810 | 0.00 | 6996 | 0.00 | 12515 | 0.70 |
| 4 | 18879 | 0.63 | 19049 | 0.86 | 7372 | 0.00 | 13995 | 0.05 |
| 5 | 18986 | 0.08 | 20323 | 0.06 | 7737 | 0.01 | 14583 | 0.02 |
| 6 | 19276 | 0.07 | 20564 | 0.07 | 7760 | 0.01 | 14889 | 0.00 |
| 7 | 21150 | 0.86 | 21222 | 0.45 | 7912 | 0.01 | 15700 | 0.00 |
| 8 | 21973 | 0.00 | 22571 | 0.00 | 8133 | 0.01 | 15866 | 0.00 |
| 9 | 23325 | 0.00 | 23399 | 0.00 | 8414 | 0.08 | 16064 | 0.01 |
| 10 | 23377 | 0.00 | 23437 | 0.00 | 9021 | 0.02 | 16320 | 0.01 |
| 11 | 23875 | 0.00 | 24599 | 0.00 | 9923 | 0.21 | 17014 | 0.00 |
| 12 | 24845 | 0.00 | 25994 | 0.00 | 10390 | 0.42 | 17829 | 0.00 |
| 13 | 25639 | 0.00 | 26521 | 0.00 | 11260 | 0.00 | 18200 | 0.01 |
| 14 | 25947 | 0.00 | 26958 | 0.00 | 11380 | 0.00 | 19203 | 0.03 |
| 15 | 26041 | 0.00 | 27024 | 0.00 | 11501 | 0.01 | 19412 | 0.00 |
| 16 | 27485 | 0.14 | 27961 | 0.14 | 12000 | 0.00 | 19608 | 1.10 |
| 17 | 28069 | 0.10 | 28004 | 0.08 | 12281 | 0.00 | 20414 | 0.00 |
| 18 | 28834 | 0.00 | 28819 | 0.00 | 12582 | 0.00 | 20717 | 0.00 |
| 19 | 29219 | 0.00 | 28888 | 0.00 | 12856 | 0.01 | 20982 | 0.07 |
| 20 | 29433 | 0.00 | 29220 | 0.00 | 13509 | 0.02 | 21177 | 0.01 |

**Table S5** Wavenumber $\tilde{\nu}$ and oscillator strength $f$ from DFT/TDDFT calculations in vacuum and acetonitrile (MeCN) for the **transitions of the radical dication H101$^{2+}$ starting from $S_0$**. "Singlet" and "Triplet" in the columns "Character" denote the character of the transition, *i.e.* if it is a $S_0 \rightarrow S_n$ or an optically dark $S_0 \rightarrow T_n$ transition, respectively.

| n | $S_0 \rightarrow S_n$ or $S_0 \rightarrow T_n$ (radical dication H101$^{2+}$) | | | | | |
|---|---|---|---|---|---|---|
| | Vacuum | | | MeCN | | |
| | $\tilde{\nu}$ / cm$^{-1}$ | $f$ | Character | $\tilde{\nu}$ / cm$^{-1}$ | $f$ | Character |
| 1 | 772 | 0.00 | Triplet | 1723 | 0.00 | Triplet |
| 2 | 7891 | 0.00 | Triplet | 8601 | 0.00 | Triplet |
| 3 | 13578 | 0.00 | Triplet | 11633 | 4.74 | Singlet |
| 4 | 13838 | 0.00 | Triplet | 13665 | 0.00 | Triplet |
| 5 | 14021 | 5.95 | Singlet | 15564 | 0.08 | Singlet |
| 6 | 14798 | 0.00 | Triplet | 16163 | 0.00 | Triplet |
| 7 | 15453 | 0.05 | Singlet | 16362 | 0.00 | Triplet |
| 8 | 17189 | 0.19 | Singlet | 16987 | 0.00 | Singlet |
| 9 | 17257 | 0.00 | Triplet | 17498 | 0.00 | Triplet |
| 10 | 17380 | 0.22 | Singlet | 18468 | 0.19 | Singlet |
| 11 | 18438 | 0.03 | Singlet | 18622 | 0.19 | Singlet |
| 12 | 18683 | 0.00 | Triplet | 19902 | 0.00 | Triplet |
| 13 | 20722 | 0.00 | Triplet | 21724 | 0.00 | Triplet |
| 14 | 21191 | 0.00 | Triplet | 21761 | 0.00 | Triplet |
| 15 | 21455 | 0.40 | Singlet | 22184 | 0.00 | Triplet |
| 16 | 21603 | 0.00 | Triplet | 22198 | 0.35 | Singlet |
| 17 | 21682 | 0.00 | Triplet | 22927 | 0.00 | Triplet |
| 18 | 21914 | 0.00 | Singlet | 23453 | 0.01 | Singlet |
| 19 | 22939 | 0.04 | Singlet | 23877 | 0.00 | Triplet |
| 20 | 23002 | 0.00 | Singlet | 24117 | 0.01 | Singlet |
| 21 | 23085 | 0.00 | Triplet | 24181 | 0.01 | Singlet |
| 22 | 23571 | 0.27 | Singlet | 24344 | 0.00 | Triplet |
| 23 | 23704 | 0.00 | Triplet | 24440 | 0.00 | Triplet |
| 24 | 23736 | 0.00 | Triplet | 24448 | 0.07 | Singlet |
| 25 | 24206 | 0.00 | Triplet | 24992 | 0.14 | Singlet |
| 26 | 24846 | 0.14 | Singlet | 25664 | 0.00 | Triplet |
| 27 | 26570 | 0.00 | Singlet | 26148 | 0.00 | Singlet |
| 28 | 26616 | 0.01 | Singlet | 26157 | 0.01 | Singlet |
| 29 | 28846 | 0.00 | Triplet | 28430 | 0.00 | Triplet |
| 30 | 29408 | 0.09 | Singlet | 29473 | 0.10 | Singlet |
| 31 | 29856 | 0.00 | Triplet | 30654 | 0.00 | Triplet |
| 32 | 30501 | 0.00 | Triplet | 30710 | 0.00 | Triplet |
| 33 | 30631 | 0.00 | Triplet | 30858 | 0.00 | Triplet |
| 34 | 30841 | 0.00 | Triplet | 31148 | 0.00 | Triplet |
| 35 | 31243 | 0.95 | Singlet | 31727 | 0.31 | Singlet |
| 36 | 33136 | 0.05 | Singlet | 34539 | 0.01 | Singlet |
| 37 | 33361 | 0.04 | Singlet | 34891 | 0.01 | Singlet |
| 38 | 33949 | 0.01 | Singlet | 35250 | 0.02 | Singlet |
| 39 | 34387 | 0.02 | Singlet | 35356 | 0.02 | Singlet |
| 40 | 34458 | 0.02 | Singlet | 35756 | 0.10 | Singlet |

# 8 References


1. U. B. Cappel, D. Moia, A. Bruno, V. Vaissier, S. A. Haque and P. R. F. Barnes, *Sci. Rep.*, 2016, **6**, 21276.
2. O. Flender, M. Scholz, J. R. Klein, K. Oum and T. Lenzer, *Phys. Chem. Chem. Phys.*, 2016, **18**, 26010.
3. S. A. Kovalenko, A. L. Dobryakov, J. Ruthmann and N. P. Ernsting, *Phys. Rev. A*, 1999, **59**, 2369.
4. F. Neese, *WIREs Comput. Mol. Sci.*, 2012, **2**, 73.
5. A. Schäfer, H. Horn and R. Ahlrichs, *J. Chem. Phys.*, 1992, **97**, 2571.
6. T. Petrenko and F. Neese, *J. Chem. Phys.*, 2007, **127**, 164319.
7. T. Petrenko and F. Neese, *J. Chem. Phys.*, 2012, **137**, 234107.